An analytical model of heat and mass transfer from liquid drops with temperature dependence of gas thermo-physical properties

G.E. Cossali*, S. Tonini
Department of Engineering and Applied Sciences, University of Bergamo
Viale Marconi 5, 24044 Dalmine (BG), Italy
*Corresponding author: gianpietro.cossali@unibg.it

April 15, 2019

Abstract

An analytical model for heating and evaporation of a single component liquid drop is developed. The model accounts for the temperature dependence of density, diffusivity, thermal conductivity and specific heat of the gas species. The effect of variable properties on heat and evaporation rates is analysed and a comparison with the prediction of the classical constant property model is reported for six different species and different operating conditions. The model allows to evaluate the effect of the choice of the gas mixture averaging parameter (the relative weight of free stream and drop surface conditions) on the prediction of the constant property model, and a way to optimise the choice is proposed. The results can be extended to non-spherical drop and examples are reported.

Nomenclature

$a_{0,1}$	coefficients for the mixture thermal conductivity (eq. 16c)	-
A	drop surface area	m^2
$A_{\alpha_{ref}}$	non-dimensional parameter (eq. 35)	-
B	incomplete beta function	-
B_M	mass transfer number	-
c	molar density	$kg/kmol$
c_h	coefficient for specific heat power law (eq. 15)	JK^{-1-b}/kg
$c_{p,v}$	vapour specific heat at constant pressure	J/kgK
d_0	coefficient for diffusivity power law (eq. 12)	$m^2K^{-7/4}/s$
D_{10}	mass diffusion coefficient	m^2/s
E_c	Eckert number $Ec = \frac{\lvert U\rvert^2}{c_{p,v}(T_\infty - T_s)}$	-
$g_{0,1};\ h_{0,1}$	constant parameters $g_p = \frac{q_p+1}{1+b};\ h_p = \frac{2+q_p-m}{1+b}$	-
H	logarithm of gas molar fraction: $H = \ln\left(y^{(0)}\right)$	-
k	thermal conductivity	W/mK
K_0	constant parameter	-
Le^M	modified Lewis number $Le^M = \frac{k_{ref}}{c_{p,v,ref}\ D_{10,ref} M_m^{(1)} c_{ref}}$	-
m_{ev}	evaporation rate	kg/s
M_m	molar mass	$kg/kmol$
$n_j^{(p)}$	mass flux of species (p)	kg/m^2s
$N_j^{(p)}$	molar flux of species (p)	$kmol/m^2s$
P	pressure	Pa
q	heat flux	W/m^2
Q	heat rate	W
r	radial distance	m
$r_{0,1}$	coefficient for the conductivity power law, (eq. 13)	WK^{-1-q_p}/m
R	universal gas constant	$J/kmolK$
R_d	drop radius	m
Sc^M	modified Schmidt number $Sc^M = \frac{\mu_{ref}}{D_{10,ref}\ c_{ref}\ M_m^{(1)}}$	-
T	temperature	K
U_j	Stefan flow velocity	m/s
y	molar fraction	-
Y	non-dimensional parameter $Y = \log\left(\frac{K_0-1}{K_0-T_s}\right)$	-
W_g	hypergeometric function $W_g(z) = {}_2F_1(g, 1, 1+g, z)$	-
z	non-dimensional variable	-

Greek symbols

α_{ref}	averaging parameter	-
γ	ratio between evaporation rates $\gamma = \frac{m^c_{ev}(\alpha_{ref})}{m_{ev}}$	-
θ	curvilinear coordinate (eq. 33)	-
Λ	non-dimensional parameter $\Lambda = \frac{RT_\infty R_d^2}{M_m^{(1)} D^2_{10,ref}}$	-
μ	viscosity	kg/ms
ξ	curvilinear coordinate (eq. 33)	-
Φ	harmonic function	-
ρ	mass density	kg/m^3
χ	mass fraction	-

Subscripts

ev	evaporation
max	maximum
mix	mixture
n	orthogonal to drop surface
obl	oblate
pl	plateau
pro	prolate
r	radial
ref	reference
s	drop surface
T	total
v	vapour
∞	ambient conditions

Superscripts

b	exponent for the specific heat power law	-
c	constant parameter model	-
m	exponent for the diffusivity power law	-
$q_{1,0}$	exponents for conductivity power laws	-
ref	at reference conditions	-
T	total	-
$\hat{}$ $\sim$	non-dimensional	-

1 Introduction

The intense study on the vaporisation of liquid droplets in gaseous environments, under way since more than a century, is motivated by the importance of this process in many industrial applications involving spray combustion, spray drying, spray cooling, fire suppression, crystallisation, painting, medical aerosol, anti-icing, etc.

Recent general reviews (see [1] and [2]) report about the large amount of research available on the field. The physical phenomena involved in this process, including phase change coupled with heat and mass transfer, can be accurately accounted for only using sophisticated numerical tools (see [3] for recent reference), but their use is limited due to the high computational costs involved. When predicting dispersed flow behaviour, simpler analytical models of heating and evaporation of liquid droplets are necessary, and the accuracy of the results are limited by many simplifying hypotheses commonly imposed by these models: drop sphericity, quasi-steadiness, constancy of the thermophysical properties, ideal gas behaviour, phase equilibrium at the interface, to cite the most common ones.

The first analytical model for drop vaporisation, assuming diffusion controlled evaporation at steady-state conditions dates back to 1877 [4], and the first inclusion of Stefan flow effect can be found in [5]. Since then, a variety of theoretical models have been developed addressing the different aspects of the phenomena involved. With respect to the assumed homogeneity of thermophysical properties, it can be noticed that in real applications like, for example, combustion chambers, the conditions are substantially non-homogeneous and the droplets may reach very different regions in terms of gaseous temperature and mixture composition. In 1975, Hubbard et al. [6] proposed a model taking into account the thermal gradients in the liquid and gas phases, with a focus on the effect of non-homogeneous thermophysical properties on the vaporisation predictions. The majority of the available analytical models of drop vaporisation (among which the most widely used is [7]) assumes that transport properties are uniform through the gas phase, then neglecting their dependence on the local temperature and composition. The values of the constant properties are evaluated by an averaging procedure, and studies available in the open literature have shown that evaporation rate predictions are quite sensitive to the choice of property values. Miller et al. [8] showed that the heat and mass fluxes between the droplet and the gaseous mixture strongly depend on the evaluation of the transport and thermodynamic properties of both the gas and the liquid phases. Sanjosé [9] confirmed that the thermodynamic and transport properties have a great impact on the evaporation process and that taking into account complex laws for them is necessary in order to perform accurate evaporation calculations, although that would increase the computational cost, not always affordable in industrial-type simulations. Hubbard et al. [6] proposed a value of this averaging parameter (the relative weight of free stream and drop surface conditions) equal to 1/3, which was found to give reasonable results under high evaporation conditions [7]. Ebrahimian et al. [10] compared the results obtained with the averaging parameter equal to 1/3 and 1/2 to experimental evaporation data, and showed that the 1/3 rule performs significantly better at high gas temperature, while at low gas temperature there is hardly any difference between the two rules. Attempts to relieve the hypothesis of homogeneous gaseous properties in theoretical models for drop evaporation appeared in the recent decades. Sirignano et al. [11] developed a generalized theory for liquid-fuel burning in arbitrary geometrical configuration with non-unitary Lewis number, introducing a

potential function that governs mass flux in the gas-phase. Sobac et al. [12] investigated the effect of homogeneous gas temperature assumption on a liquid spherical drop evaporating in stagnant air. The local dependence of the physicochemical properties on the gas temperature was considered, proposing a numerical solution for the mass and energy conservation equations under quasi-steady conditions. The authors of the present work partially addressed this issue, proposing an analytical solution to the energy and species conservation equations, accounting for the local dependence of the gaseous mixture density on the temperature, for a single spherical drop [13] and for two interacting spherical drops [14]. The model was then extended, for the case of a single spherical drop, accounting for the dependence on temperature of both the gas density and the diffusion coefficient [15]. In [16], an analytical model that accounts for temperature dependence of gas conductivity and diffusivity coefficients was proposed, using the same power law dependence for both properties. As already pointed out, almost all analytical models available in the open literature assumes a spherical shape for the evaporating drop. However, experimental observations (see [17]) show that in dispersed phase scenarios, liquid drops are far from being spherical. A droplet moving in a gas medium is prone to dynamic stresses on the droplet surface [18]; while the gas dynamic stress forces the droplet to deform, the surface tension tends to minimise the interface area, which leads to a spherical shape [19]. At a Weber number much higher than unity, droplet shape deviates from sphericity [20], furthermore time-dependent drop/gas interaction might induce the droplet shape to oscillate [21], and spheroidal shapes are found to be good approximation of non-spherical particles [22]. Recently [23] proposed a theoretical and experimental study for the evaporation of an acoustically levitated oblate liquid droplet. The evaporation rate of the liquid droplet was measured experimentally, revealing that evaporation of spheroidal droplets follows the well-known d^2-law [24]. *To take into account the effect of non-spherical shapes of evaporating drops,* a *universal scaling law was recently proposed, for sessile drops, by [25], to correlate the evaporation flux with local drop curvatures.* Analytical models of the heat and mass transfer from spheroidal [26], [27] and triaxial drops [28] were proposed for single component drops, recently extended to multi-component ellipsoidal drops in [29]. All the above discussed analytical models assume constant properties of the gaseous phase.

The present work reports a fully analytical solution of the species and energy conservation equations for single component drops evaporating in stagnant environment, accounting for the temperature dependence of density, diffusion coefficient, specific heat and thermal conductivity of the gaseous species and extending the solution to non-spherical shapes.

The next sections describe the mathematical model, followed by the analysis on the effect of temperature dependence of thermophysical properties on heat and mass transfer, suggesting simple correlation for the averaging coefficient that could be implemented in CFD codes for dispersed phase applications.

2 Mathematical model

The analytical model reported below describes the heat and mass transfer from a single component evaporating drop to a quiescent gaseous environment, under quasi-steady conditions. The dependence on the temperature of density,

thermal conductivity, diffusion coefficient and specific heat capacity of the gaseous species will be taken into account by assuming simplified dependences (namely, power laws), which will be justified in the next section against available data. The steady-state energy, momentum and species conservation equations will be written for general shapes of the evaporating drop, and analytical solutions will be reported.

The species conservation equations, under quasi-steady assumption, are:

$$\nabla_j N_j^{(p)} = 0 \qquad p = (0,1) \tag{1}$$

where

$$N_j^{(p)} = N_j^{(T)} y^{(p)} - cD_{10} \nabla_j y^{(p)} \tag{2}$$

are the molar fluxes. The index $p = (0,1)$ stands for the gas *(which can be a mixture of gases)* and the evaporating species, respectively. $y^{(p)}$ is the molar fraction of the species p, $N_j^{(T)} = N_j^{(1)} + N_j^{(0)}$ and c is the molar gas density. Assuming ideal gas behaviour, the molar gas density is:

$$c = \frac{P_T}{RT} \tag{3}$$

The molar form of the species conservation equations (1, 2) will be used here since it was shown [30] that, for single component drops, it is equivalent to the more often used mass form [5], [7], and mass fluxes can be obtained from molar fluxes by $n_j^{(p)} = N_j^{(p)} Mm^{(p)}$. The simplification in using the molar form is mainly related to the observation that the mass density depends also on gas composition; for an ideal binary mixture:

$$\rho = \frac{P_T Mm^{(0)}}{RT} \left(1 + \frac{Mm^{(1)} - Mm^{(0)}}{Mm^{(0)}} y^{(1)} \right) \tag{4}$$

and this yields less simpler form of the analytical solutions when compared to those obtained from the molar approach (see [30] for more details).

Assuming that the diffusion of the component $p = 0$ into the liquid drop is neglectful (i.e. pure liquid) and a stationary liquid-gas interface, the flux of this component is zero everywhere, and the first of equations (2) yields:

$$N_j^T = cD_{10} \nabla_j H \tag{5}$$

where $H = \ln y^{(0)}$. Mass conservation equation is obtained summing equations (1):

$$\nabla_j \left(\rho U_j \right) = 0 \tag{6}$$

and, since under the mentioned assumptions: $\rho U_j = n_j^T = n_j^{(1)} = M_m^{(1)} N_j^T$, equations (6) and (5) yield:

$$\nabla_j \left(M_m^{(1)} cD_{10} \nabla_j H \right) = 0 \tag{7}$$

To notice that, since equations (1), (2) and (6) are not independent, one of the species conservation equation can be disregarded.

The heat transfer from the evaporating drop is described by the following simplified form of the energy equation:

$$c_{p,v} \rho U_j \nabla_j T = \nabla_j \left(k \nabla_j T \right) \tag{8}$$

where inter-diffusional terms are considered as in [31], while dissipation by viscous stress is neglected since the Eckert number $Ec = \frac{|U|^2}{c_{p,v}(T_\infty - T_s)}$ is very small for large temperature differences and further minor terms (refer to [32] p. 465, or [33] p. 589, for a more complete form of the equation) are neglected. Thermal conductivity k and specific heat capacity $c_{p,v}$ are assumed to depend on temperature. Substituting (5) into (8) yields:

$$c_{p,v} M m^{(1)} c D_{10} \nabla_j H \nabla_j T = \nabla_j \left(k \nabla_j T \right) \tag{9}$$

The momentum conservation equation can be written, under the same simplifying hypotheses and assuming constant shear viscosity and neglectful bulk viscosity, as [13]:

$$\rho U_j \nabla_j U_k = -\nabla_k P_T + \mu \nabla^2 U_k \tag{10}$$

2.1 Dependence of gas thermophysical properties on temperature

When analytical solutions of the above reported conservation equations are searched, a typical assumption is that of constant properties. All the relevant properties of the gaseous species and the mixture are then assumed to maintain the value calculated at a reference temperature (and composition). It has been often noticed [8], [10] that the prediction of such models show an important dependence on the reference conditions, which are defined as:

$$T_{ref} = \alpha_{ref} T_\infty + (1 - \alpha_{ref}) T_s \tag{11a}$$

$$\chi^{(p)}_{ref} = \alpha_{ref} \chi^{(p)}_\infty + (1 - \alpha_{ref}) \chi^{(p)}_s \tag{11b}$$

where α_{ref} is the averaging parameter. The correct choice of α_{ref} has been matter of debate and it is usually assumed to be equal to 1/2 or to 1/3 [10].

The novelty of the present analytical approach relies on the fact that analytical solutions of the conservation equations will be presented accounting for temperature dependence of gas molar density (c), binary mass diffusion coefficient (D_{10}), mixture thermal conductivity (k_{mix}) and vapour specific heat capacity ($c_{p,v}$), with the aim of mitigating this problem. As above stated, the temperature and pressure dependence of molar gas density is that found for an ideal gas (equation 3). The binary diffusion coefficient D_{10} is assumed to depend on temperature following the general rule:

$$D_{10} = d_0 \frac{T^m}{P_T} \tag{12}$$

where d_0 is a constant. Classical statistical thermodynamics suggests a temperature dependence of the proposed form where $m = 3/2$ [34], while $m = 7/4$ is the value assumed in the widely used Fuller-Schettler-Giddings (FSG) correlation [35].

The thermal conductivity of a pure gaseous substance p is also approximated by a power law:

$$k^{(p)} = r_p T^{q_p} \tag{13}$$

and this is consistent with the results of Chapman-Enskog treatment for monoatomic gases at low density [36], where $q_p = 1/2$. For polyatomic gases the temperature dependence modifies, the Eucken formula [37] can be used, but the temperature correlation (13) is still usable, with different values of q_p (see section 3.1.1).

The conductivity of the gas vapour mixture (k_{mix}) can be evaluated from the conductivities of the pure substances $\left(k^{(p)}\right)$ by different methods, here the Wassiljewa [38] relation, *which is commonly used to predict the thermal conductivity values of gas mixtures for low pressure, was chosen due to the simple linear dependence of the gas mixture conductivity on the values of the pure species*:

$$k_{mix} = \frac{k^{(0)} y_{ref}^{(0)}}{y_{ref}^{(0)} + A_{01} y_{ref}^{(1)}} + \frac{k^{(1)} y_{ref}^{(1)}}{y_{ref}^{(1)} + A_{10} y_{ref}^{(0)}} \tag{14}$$

and the coefficients A_{jk} are obtained from the Lindsay and Bromley relationship [39], neglecting their temperature dependence.

The temperature dependence of vapour heat capacity on temperature at low pressure is often described by polynomials or power series [40]. For the purpose of the following analytical approach the assumed dependence will be

$$c_{p,v} = c_h T^b \tag{15}$$

where the constants c_h and b are found by data fitting. A deeper analysis of the error introduced by this assumption is reported in the following section.

2.1.1 Accuracy of power law assumption

The temperature dependence of specific heat at constant pressure and thermal conductivity of pure vapours are approximated by power laws (see equations 15, 14) and the coefficients r_j, q_j, c_h, b were evaluated by fitting available databases [41], with the exception of the acetone thermal conductivity, where the power law was fitted to the data calculated using Misic and Thodos method [42].

Low pressure values have been used for this fitting, consistently with the assumed ideal gas behaviour and table 1 reports the values of the coefficients for the species used in the present study. The average difference between the fitted curve and the data is, for the chosen species, lower than 1.5% for the specific heat values and lower than 3.2% for the thermal conductivity.

While the assumption of low vapour pressure may be acceptable far from the drop surface, where vapour concentrations are low, some inconsistencies can be expected when using these correlations to approximate the thermophysical properties close to the surface of the evaporating drops, particularly under high evaporation conditions, since in that cases the vapour pressure may be relatively high. When evaporating in a *quiescent hot* environment, a drop heats up to what is often called the "plateau" temperature, which depends on the species and the gas temperature, and remains at that temperature for almost the whole drop lifetime (see [2]). To assess the accuracy of the proposed correlations, the values predicted by equations (14) and (15) using the coefficients of table 1 were compared with data at vapour pressures equal to the saturation pressure of each species at plateau temperature (T_{pl} reported in table 2), estimated for spherical drops evaporating in quiescent atmosphere. The results reported in table 2, as percentage difference with respect to the value at saturation conditions, show that for all the chosen species the discrepancies for the estimation of the thermal conductivity remain below 2%, with the exception of acetone for which the discrepancy

reaches a maximum of 5.3% at the highest temperature. The same happens for the discrepancies between the values of the specific heat for ethanol, n-hexane, n-octane and n-dodecane. For water and acetone, specific heat discrepancies may get close to 5% and 8%, respectively (at high gas temperature). It should be remarked that the maximum differences may be reached only in a relatively small region close to the drop surface, where vapour concentration is higher, but they become negligible in all the remaining space.

Table 1.

Coefficients for the evaluation of thermophysical properties (vapour heat capacity, thermal conductivity and binary diffusion coefficient) for different species.

	c_h $[J\ Kg^{-1}K^{-1-s}]$	b $\left[W\ m^{-1}K^{-1-p_1}\right]$	r_p $[WK^{-1-q_p}/m]$	q_p $[-]$	d_0 $[m^2s^{-1}K^{-1.75}]$
Species	eq. (15)	eq. (15)	eq. (13)	eq. (13)	eq. (12)
water	822.34	0.14135	6.96×10^{-6}	1.3767	1.20×10^{-9}
acetone	29.024	0.66874	1.36×10^{-6}	1.5965	5.13×10^{-10}
ethanol	57.325	0.58516	1.04×10^{-6}	1.6963	6.03×10^{-10}
n-hexane	24.504	0.74308	5.46×10^{-7}	1.7765	3.59×10^{-10}
n-octane	24.96	0.73904	2.71×10^{-7}	1.869	3.07×10^{-10}
n-dodecane	25.756	0.73309	1.74×10^{-7}	1.9047	2.48×10^{-10}
air	–	–	2.99×10^{-4}	0.7871	–

Table 2

Liquid plateau temperature, T_{pl}, as function of gas temperature for different species and corresponding percentage difference of vapour heat capacity, $\Delta c_{p,vap}\%$, and thermal conductivity, $\Delta k^{(1)}\%$, predicted by equations (15) and (14) with respect to the value at saturation conditions.

	$T_\infty = 500K$			$T_\infty = 1000K$		
species	T_{pl}	$\Delta c_{p,vap}\%$	$\Delta k^{(1)}\%$	T_{pl}	$\Delta c_{p,vap}\%$	$\Delta k^{(1)}\%$
water	317.1	−2.98	−0.85	339.5	−4.82	−1.99
acetone	291.8	−4.62	−2.79	308.5	−7.77	−5.32
ethanol	311.4	−0.11	−0.17	329.0	−0.79	−0.43
n-hexane	305.4	−1.06	−0.36	322.0	−1.74	−0.67
n-octane	351.4	−0.87	−0.54	372.7	−1.40	−0.96
n-dodecane	418.7	−0.46	−0.84	452.5	−0.92	−1.92

2.2 Boundary conditions

The conservation equations (7), (9) and (10) are rather general and independent of shape and position of the evaporating surfaces, which are described by proper forms of the boundary conditions.

The temperature boundary condition at infinite distance from the drop is assumed uniform and equal to the constant value T_∞ while on the drop surface it is assumed uniform and equal to T_s. The species boundary conditions are defined by the value of the molar fraction at infinity ($y_\infty^{(p)}$) which may be chosen arbitrarily, and that on the surface, which is defined by the surface temperature since equilibrium conditions are assumed.

2.3 Non-dimensional form of the conservation equations

The conservation equations, the boundary conditions and the temperature dependence of the thermophysical properties can be conveniently non-dimensionalised. A general reference temperature T_{ref} will be used here to evaluate the main nondimensional constants but it will be shown that such a choice does not influence the prediction of the model. The following non-dimensional quantities will be used: the non-dimensional temperature ($\hat{T} = \frac{T}{T_\infty}$), velocity ($\tilde{U} = U\frac{R_d}{D_{10}}$) and pressure ($\tilde{P}_T = \frac{P_T}{c_{ref}\bar{R}T_\infty}$), the modified Schmidt number ($Sc^M = \frac{\mu_{ref}}{D_{10,ref}\ c_{ref}\ M_m^{(1)}}$) and modified Lewis number ($Le^M = \frac{k_{ref}}{c_{p,v,ref}\ D_{10,ref}M_m^{(1)}c_{ref}}$) and the parameter $\Lambda = \frac{\bar{R}T_\infty R_d^2}{M_m^{(1)}D_{10,ref}^2}$, where R_d is the equivalent drop radius, i.e. the radius of a spherical drop having the same volume of the actual drop. In this paragraph, the non-dimensional "nabla" operator is defined as $\hat{\nabla}_j = R_d\nabla_j$. The reference temperature T_{ref} is assumed to evaluate the constants in equations (12),(13) and (15), yielding the following relationships:

$$D_{10} = D_{ref}T_{ref}^{-m}T^m = D_{ref}\hat{T}_{ref}^{-m}\hat{T}^m \tag{16a}$$

$$c = c_{ref}T_{ref}T^{-1} = c_{ref}\hat{T}_{ref}\hat{T}^{-1} \tag{16b}$$

$$k_{mix} = k_{ref}\frac{a_0\hat{T}^{q_0} + a_1\hat{T}^{q_1}}{a_0\hat{T}_{ref}^{q_0} + a_1\hat{T}_{ref}^{q_1}} \tag{16c}$$

$$c_{p,v} = c_{p,v,ref}T_{ref}^{-b}T^b = c_{p,v,ref}\hat{T}_{ref}^{-b}\hat{T}^b \tag{16d}$$

It is worth to stress again that the choice of T_{ref} is completely arbitrary, then the averaging parameter α_{ref}, used to evaluate the reference conditions, does not influence the values of these properties. But the mixture conductivity is influenced also by composition, and this dependence is accounted for by using the reference composition (equation 11b). Then the choice of the averaging parameter α_{ref} is expected to slightly influence the predictions of the model, and this will be shown in a following section.

The energy equation (9) becomes:

$$\left(\hat{T}^{m-1+b}\nabla_j\hat{H}\right)\hat{\nabla}_jT = \hat{\nabla}_j\left[\left(a_0\hat{T}^{q_0} + a_1\hat{T}^{q_1}\right)\hat{\nabla}_jT\right] \tag{17}$$

where $\hat{H} = H\frac{\left(a_0\hat{T}_{ref}^{q_0} + a_1\hat{T}_{ref}^{q_1}\right)\hat{T}_{ref}^{1-m-b}}{Le^M}$, while equation (7) becomes:

$$\hat{\nabla}_j\left(\hat{T}_j^{m-1}\hat{\nabla}_j\hat{H}\right) = 0 \tag{18}$$

The momentum conservation equation (10) can also be written in non-dimensional form as:

$$\hat{\nabla}_k \tilde{P}_T = \frac{1}{\Lambda}\left[Sc^M \hat{\nabla}^2 \tilde{U}_k - \tilde{P}_T \tilde{T}^{-1} \hat{\nabla}_j H \hat{\nabla}_j \tilde{U}_k\right] \tag{19}$$

and it has been shown, [13] and [43], that the non-dimensional parameter Λ becomes quite large for a large variety of conditions of interest for applications. This observation justifies the use of an asymptotic form (for $\Lambda \to \infty$), that in the present case yields: $\hat{\nabla}_k \tilde{P}_T = 0$ and then $\tilde{P}_T = const.$ The constancy of P_T allows to disregard the dependence of the thermophysical properties on the pressure, although, when calculations are performed, the correct values of the constants in equations (12),(13) and (15) at the given pressure can be used.

2.4 Analytic solution of the conservation equations

The analytic solution of the non-linear partial differential equation (PDE) system (17) and (18) can be found introducing an auxiliary harmonic function Φ (i.e. $\nabla^2 \Phi = 0$) equal to 1 over the drop surface and zero at infinity. This approach was introduced by Laboswky [44] and later used by many authors to solve similar problems [45], [11]. The details of the solution procedure can be found in the Appendix, where it is shown that defining:

$$W_g(x) = {}_2F_1(g, 1, 1+g, x) \tag{20}$$

where ${}_2F_1(a, b, c, x)$ is the hypergeometric function (see [46] for the properties) the function $\hat{H}$ and $\hat{T}$ can be written in implicit form as (see equations A.6 and A.8):

$$\hat{H} = -\frac{1}{K_0}\left[\frac{a_0 \hat{T}^{q_0-m+2}}{h_0} W_{h_0}\left(\frac{\hat{T}^{1+b}}{K_0}\right) + \frac{a_1 \hat{T}^{q_1-m+2}}{h_1} W_{h_1}\left(\frac{\hat{T}^{1+b}}{K_0}\right)\right] + \hat{H}_0 \tag{21a}$$

$$\Phi = \Phi_1\left[a_0 \frac{\hat{T}^{q_0+1}\, W_{g_0}\left(\frac{\hat{T}^{1+b}}{K_0}\right)}{K_0(q_0+1)} + a_1 \frac{\hat{T}^{q_1+1}\, W_{g_1}\left(\frac{\hat{T}^{1+b}}{K_0}\right)}{K_0(q_1+1)}\right] + \Phi_0 \tag{21b}$$

The constant K_0 appearing in these equations can be calculated by solving the trascendental equation:

$$\hat{H}_\infty - \hat{H}_s = a_0 X_0 + a_1 X_1 \tag{22}$$

obtained by taking the difference of equations (A.7a) and (A.7b), and defining:

$$X_j = \frac{\hat{T}_s^{q_0-m+2}}{K_0 h_j} W_{h_j}\left(\frac{\hat{T}_s^{1+b}}{K_0}\right) - \frac{1}{K_0 h_j} W_{h_j}\left(\frac{1}{K_0}\right) \tag{23}$$

Once K_0 is known, the other constants $\hat{H}_0$, Φ_0, Φ_1 can be found solving the linear system (A.7a, A.7b, A.9a, A.9b), satisfying all the boundary conditions.

2.5 Heat and evaporation rates

The vapour mass flux component normal to the drop surface can be evaluated from equations (2), (21a) and (A.13) as:

$$n_{s,n}^{(1)} = M_m^{(1)} c D_{10} \nabla_n H = -\frac{k_{ref} \hat{T}_{ref}^s (1+b)}{c_{p,v,ref}\left(a_0 \hat{T}_{ref}^{q_0} + a_1 \hat{T}_{ref}^{q_1}\right)\Phi_1} \nabla_n \Phi \tag{24}$$

while the heat flux normal to the drop surface is:

$$q_{s,n} = -k_{mix}\left(T_s\right)\nabla_n T = -T_\infty \frac{k_{ref}\left(K_0 - \hat{T}_s^{1+b}\right)}{\Phi_1\left(a_0\hat{T}_{ref}^{q_0} + a_1\hat{T}_{ref}^{q_1}\right)}\nabla_n\Phi \tag{25}$$

where equation (A.12b) was used.

It is interesting to notice that the effect of drop geometry on heat and mass fluxes is given by the gradient $\nabla_n\Phi$, which is independent of the thermophysical properties, while the effect of the properties and operating conditions is contained into the multipliers of $\nabla_n\Phi$ in equations (24) and (25), and they do not depend on the geometry of the problem.

The evaporation rate and the heat rate can be calculated by integrating the local fluxes over the drop surface:

$$m_{ev} = \int_A n_{s,n}^{(1)} dA = -\frac{k_{ref}\hat{T}_{ref}^{s}\left(1+b\right)}{c_{p,v,ref}\left(a_0\hat{T}_{ref}^{q_0} + a_1\hat{T}_{ref}^{q_1}\right)\Phi_1}\int_A \nabla_n\Phi dA \tag{26a}$$

$$Q = \int_A q_{s,n} dA = -T_\infty \frac{k_{ref}\left(K_0 - \hat{T}_s^{1+b}\right)}{\Phi_1\left(a_0\hat{T}_{ref}^{q_0} + a_1\hat{T}_{ref}^{q_1}\right)}\int_A \nabla_n\Phi dA \tag{26b}$$

It is worth to notice that the results obtained in this section can be used to model heating and evaporation for any drop shapes as far as the function Φ is known. Example for non-spherical drops will be reported in the following section.

3 Results and discussion

Previous attempts to relieve the condition of constant properties can be seen as a special case of the present model, since each of them can be obtained by a proper choice of the coefficients m, b, q_j. The constant properties model can be obtained by setting $[m, b, q_0, q_1] = [1, 0, 0, 0]$ although in this case the version with constant molar density (instead of constant mass density) is obtained, see [30] for a discussion about the two versions. Choosing $[m, b, q_0, q_1] = [0, 0, 0, 0]$ the variable density model, proposed in [13] and [30] for spherical drops and in [14] for pair of drops, is obtained. In this case, since $g_p = 1$ and $h_p = 2$, the functions W_g become (see [46]):

$$W_1\left(z\right) = {}_2F_1\left(1, 1, 2, z\right) = -\frac{1}{z}\log\left(1-z\right) \tag{27a}$$

$$W_2\left(z\right) = {}_2F_1\left(2, 1, 3, z\right) = -\frac{2\left(z + \log\left(1-z\right)\right)}{z^2} \tag{27b}$$

Equation (21b) and the boundary conditions (A.7b, A.7a) yield the following explicit form of the temperature field:

$$\hat{T} = K_0 - e^{-\Phi Y}\left(K_0 - 1\right) \tag{28}$$

where $Y = \log\left(\frac{K_0 - 1}{K_0 - \hat{T}_s}\right)$. For the case of a spherical boundary, the harmonic function Φ is:

$$\Phi = \frac{R_0}{r} \tag{29}$$

and then

$$\int_A \nabla_n \Phi dA = -4\pi R_0 \tag{30}$$

Equation (26a) yields the evaporation rate:

$$m_{ev} = 4\pi R_0 \frac{k_{ref}}{c_{p,v,ref}} Y \tag{31}$$

and equation (28) is then equivalent, for the spherical case ($K_0 = \frac{\hat{T}_s - e^{-Y}}{1-e^{-Y}}$), to equation (8) in [13] and equation (4) in [15], while in [30] the same equation (equation 9) is reported with the coefficient of the exponential term erroneously exchanged with the constant term. The actual value of the constant K_0 can be calculated from equations (A.13) that, using (27b), reduces to:

$$\ln\left(\frac{1-y_{v,\infty}}{1-y_{v,s}}\right)\frac{\hat{T}_{ref}}{Le^M} = \left[1 - \hat{T}_s + K_0 \log\left(\frac{K_0 - 1}{K_0 - \hat{T}_s}\right)\right] \tag{32}$$

which is equivalent to equations (18,19) in [30].

For pair of drops the function Φ assumes a more complex form, (see for example [44] or equation (22) in [14]), but the same procedure above reported can be used to re-obtain all the results.

Choosing $m \neq 0$ and $[b, q_0, q_1] = [0, 0, 0]$ the model proposed in [15] for spherical drops is obtained, where both gas density and diffusion coefficient were assumed to depend on temperature. The two cases considered there, namely $m = \frac{3}{2}$ as suggested by classical statistical physics [34] and $m = 1.75$ given by the widely used FSG correlation [35], can then be obtained following a procedure similar to that above shown.

Extension of these results to non-spherical drops is now straightforward. For example, considering spheroidal drops, the surface can be defined in spheroidal coordinates (see [27] for more details):

$$\begin{array}{cc} x = a\sinh(\xi)\sin(\theta)\cos\varphi & x = a\cosh(\xi)\sin(\theta)\cos\varphi \\ y = a\sinh(\xi)\sin(\theta)\sin\varphi & y = a\cosh(\xi)\sin(\theta)\sin\varphi \\ z = a\cosh(\xi)\cos(\theta) & z = a\sinh(\xi)\cos(\theta) \\ \text{Prolate} & \text{Oblate} \end{array} \tag{33}$$

as $\xi = \xi_0$ where ξ_0 is a constant. The corresponding form of the harmonic function Φ in such coordinates is given by (see also [47]):

$$\begin{array}{cc} \Phi_{pro} = \frac{\ln\left(\frac{e^{\xi}-1}{e^{\xi}+1}\right)}{\ln\left(\frac{e^{\xi_0}-1}{e^{\xi_0}+1}\right)} & \Phi_{obl} = \frac{2\arctan(\sinh\xi)-\pi}{2\arctan(\sinh\xi_0)-\pi} \\ \text{Prolate} & \text{Oblate} \end{array} \tag{34}$$

For the case of constant properties, an explicit form for the temperature and vapour molar fraction fields can be obtained from equations (21b) and (A.6), following the same procedure as for the spherical case. For example, the temperature field is again given by equation (28), which is exactly the results reported in [27], page 239. For the variable properties case the explicit form for temperature and vapour fields may not exist, since it depend on the reversibility of the functions $W_g(z)$, however the heat and evaporation fluxes can still be explicitly calculated from equations (25) and (24), and the heat and the evaporation rates from equations (26b) and (26a).

4 Effect of reference conditions

This section reports the analysis of the effect of reference conditions on the evaporation characteristics, as predicted by the analytical model described in the previous paragraph and by the "classical" model, which imposes constant physical properties at reference mixture temperature and vapour mass fraction using the averaging parameter α_{ref} (see equation 11b). *In the present investigation the gaseous mixture is assumed to be an ideal mixture of air and the evaporating species.* According to the literature, the drop vaporisation rate is "extremely sensitive to the method used for the evaluation of the physical properties" [7]. As an example of such sensitivity, Figure 1 reports the ratio between the evaporation rate calculated by the constant property model using $\alpha_{ref} = 1/3$ (as proposed in [48]) and the corresponding evaporation rate using the "classical" value $\alpha_{ref} = 1/2$. The ratio is reported as function of the drop temperature and two gas temperatures at free stream conditions, equal to 500 K and 1000 K, for water and n-dodecane drops. The results show that, for water drops (Figure 1a), the evaporation rate predicted using $\alpha_{ref} = 1/3$ is about 7% and 15% lower than the one predicted using $\alpha_{ref} = 1/2$ at gas temperature equal to 500 K and 1000 K, respectively. The differences are even more evident for n-dodecane drops, particularly at high liquid temperature, where the evaporation rate predicted using α_{ref} equal to 1/3 is about 25% and 15% higher than the one predicted using α_{ref} equal to 1/2 at gas temperature equal to 500 K and 1000 K, respectively. Interestingly, the results for n-dodecane (Figure 1b) evidence that at liquid temperature around 390 K ($T_\infty = 500K$) and 430 K ($T_\infty = 1000K$) the ratio approaches 1, suggesting that under these conditions the evaporation rate may become independent on the choice of the averaging parameter. *These results reflect the behaviour of the averaging parameter α_{ref} as function of the temperature for the two selected species, which varies from 1/2 down to about 1/3 for water increasing the temperature from 280 K up to the boiling temperature, while for n-dodecane α_{ref} spans within a larger interval from 1/2 down to about 0.15 as the temperature varies from 280 K up to the species boiling value.*

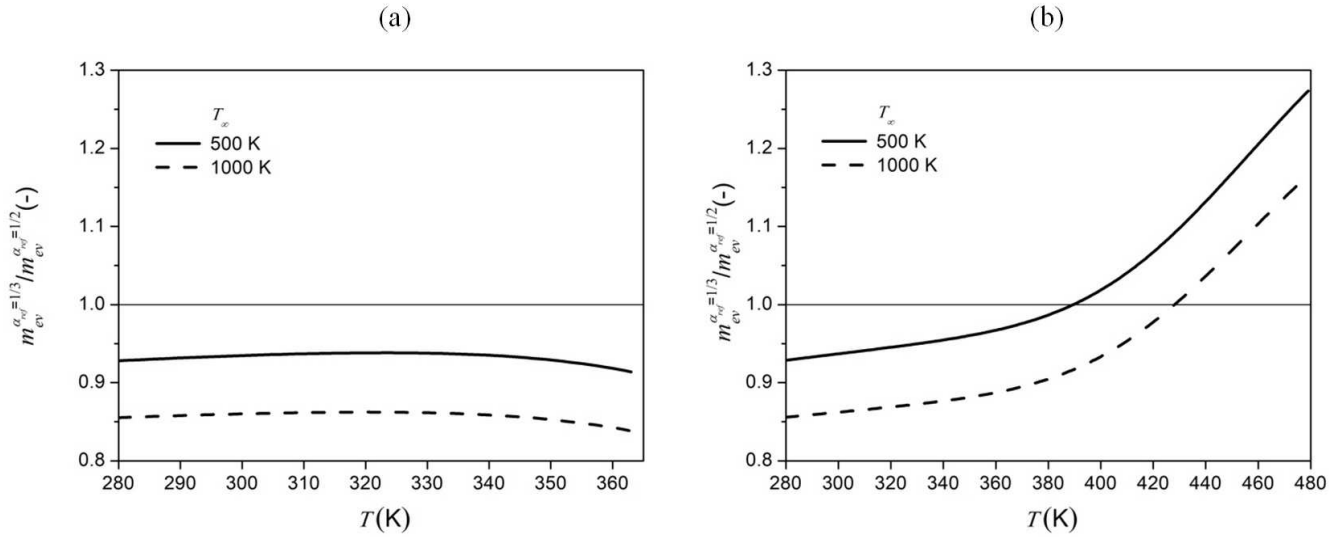

Figure 1. Effect of averaging parameter α_{ref} on the evaporation rate ratio predicted by the constant property model, as function of drop temperature at two gas temperatures, for (a) water and (b) n-dodecane drop.

A substantial different behaviour is obtained with the present model, which solves the species and energy conservation equations accounting for the explicit dependence on temperature of density, diffusivity, conductivity and specific heat of the gas species, while the mixture composition is taken into account when calculating the gas mixture thermal conductivity by imposing a reference composition with a constant valued of the averaging parameter α_{ref} . The effect of changing this constant value for the averaging parameter α_{ref} in the predictions from the present model is shown in figure 2, which reports, as above, the ratio between the evaporation rate using $\alpha_{ref} = 1/3$ and the evaporation rate using $\alpha_{ref} = 1/2$. The results are again reported as function of the drop temperature and for two gas temperatures at free stream conditions (namely 500 K and 1000 K) for water and n-dodecane drops. As expected, the dependence on α_{ref} is weak; almost negligible at lower drop temperature, it slightly increases reaching the maximum value when the drop approaches the boiling condition, but the differences remain below 2% for water (Figure 2a) and 4.5% for n-dodecane (Figure 2b) for gas temperature equal to 500 K. This effect is even reduced for higher gas temperature. A similar trend can be detected for other selected species vaporising in air (not shown here), with the largest effect detected for acetone and n-octane drops for drop temperature close to boiling and gas temperature equal to 500 K (discrepancies about 6%, *which is of the same order of the results shown here*).

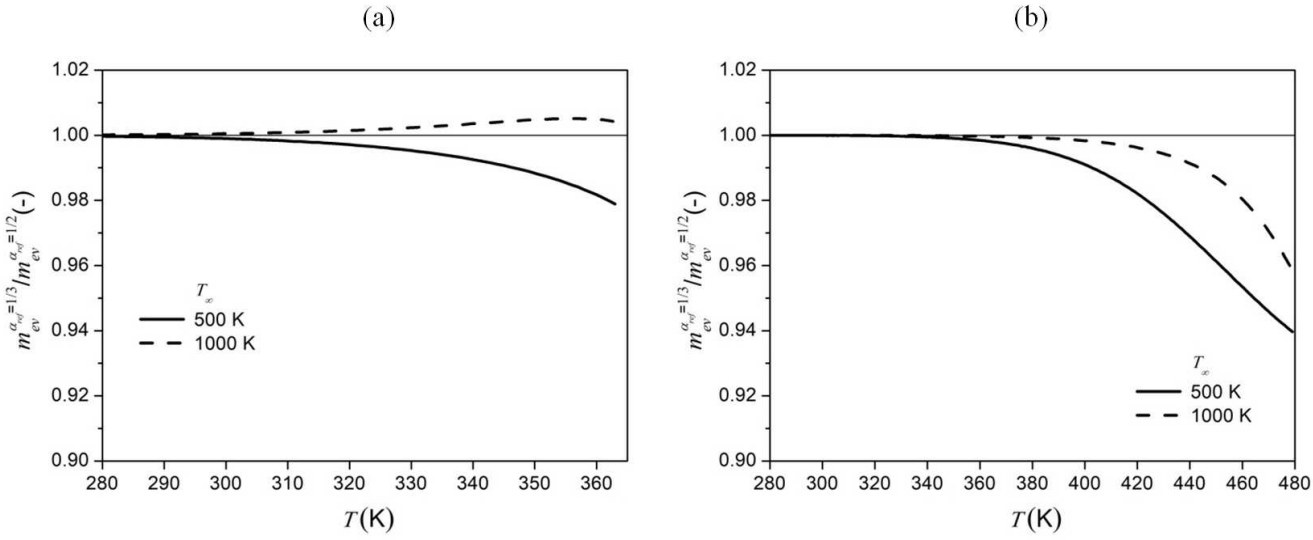

Figure 2. Effect of averaging parameter α_{ref} on the evaporation rate ratio predicted by the present variable property model, as function of drop temperature at two gas temperatures, for (a) water and (b) n-dodecane drop.

This analysis shows that the present model is, as expected, weakly dependent on the effect of reference conditions *and for the following study the value of 1/2 has been chosen.* A similar investigation was performed considering the heat rate (see equation 26b) instead of the evaporation rate, and the results (not reported here) *show the same* findings.

The effect of the averaging parameter α_{ref} on the prediction of the evaporation rate from the classical constant property model is further investigated. The ratio γ between the evaporation rate predicted by the constant property model ($m_{ev}^c(\alpha_{ref})$), using a selected α_{ref}, and the evaporation rate predicted by the present model (m_{ev}), which

is almost independent on the choice of α_{ref} (see above), i.e. $\gamma = \frac{m^c_{ev}(\alpha_{ref})}{m_{ev}}$, is evaluated as a function of drop temperature and for two values of gas temperature (500 K and 1000 K). It is worth to stress again that this ratio (see equation 26a) is independent of the drop shape, which is accounted for only by the function Φ.

Figure 3a,b reports the profiles of γ as function of the drop temperature, with six values of the averaging parameter, between 0.1 and 0.6, for water drops evaporating in air at 500 K (figure 3a) and 1000 K (figure 3b). The results show that, for drop temperature lower than 340K ($T_\infty = 500K$) and 304K ($T_\infty = 1000K$), the value of γ approaches 1 when α_{ref} is around 1/2 (the difference is lower then 1%), while at larger drop temperatures γ becomes closer to one for lower values of α_{ref}: for drop temperature close to the boiling point the value $\alpha_{ref} = 0.4$ is giving the best agreement.

However, these findings cannot be extended to other species. Figure 3c,d reports an analysis for n-dodecane drops similar to the previous one. Again, there is a drop temperature interval where the constant property model (with $\alpha_{ref} = 1/2$) predicts results close to those given by the new model (with discrepancies lower than 1%): $T_s < 390K$ for T_∞ =500K and $T_s < 415K$ for $T_\infty = 1000K$. However, the figure shows that, when the drop temperature is around 390 K ($T_\infty = 500K$) and 430 K ($T_\infty = 1000K$), none of the selected values for α_{ref} allow to reach $\gamma = 1$, i.e. the two models cannot yield the same prediction, whatever the averaging parameter is, but the same value of γ (0.997 at $T_\infty = 500K$ and 0.97 at $T_\infty = 1000K$) is obtained, almost independently of α_{ref}. A similar behaviour can be detected with other selected species (acetone, ethanol, n-hexane, n-octane), although the interval of drop temperatures corresponding to the cases where no value of α_{ref} predicts γ to be equal to 1 varies according to the

gas temperature and the species.

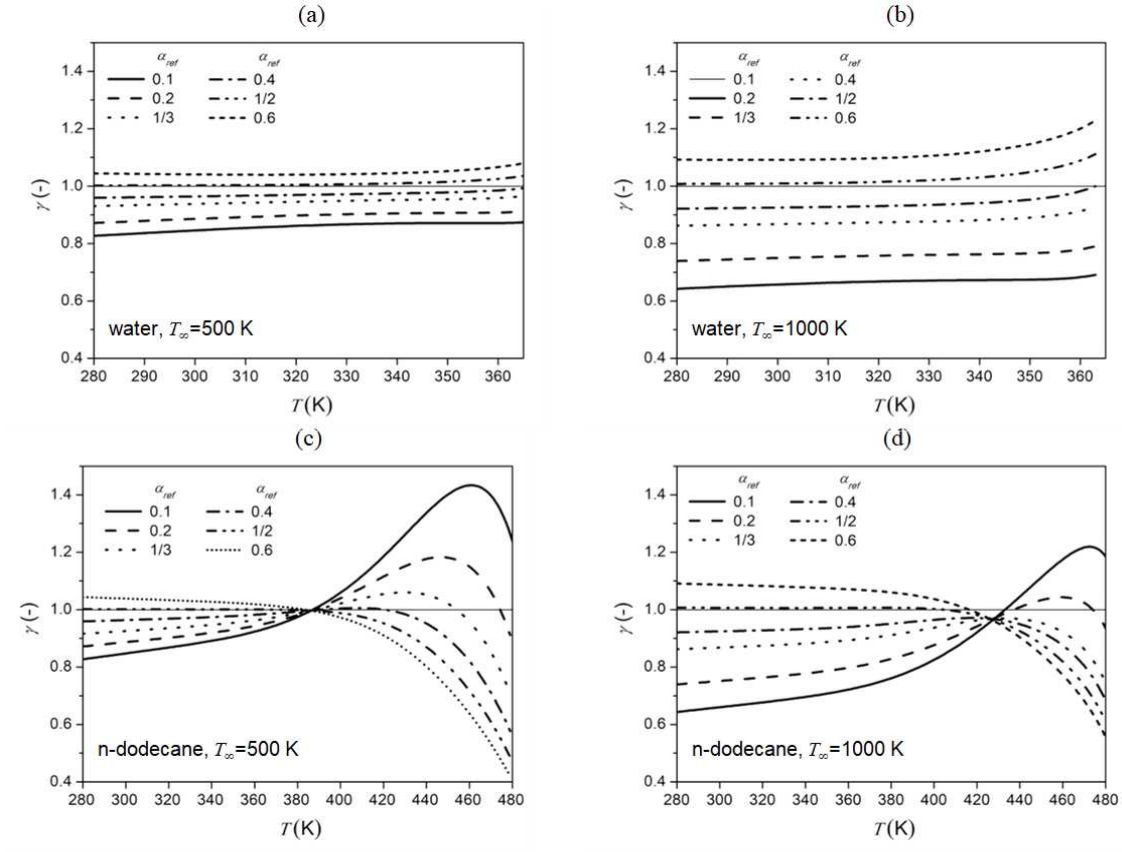

Figure 3. Evaporation rate ratio γ as function of liquid temperature, for different averaging parameter α_{ref} in the constant gas density model, for water drops at (a) 500 K and (b) 1000 K gas temperature and for n-dodecane drops at (c) 500 K and (d) 1000 K gas temperature.

4.1 Optimal value of the averaging coefficient

The analysis reported in the previous section hints the following consideration: assuming that the model accounting for the full dependence on temperature of the thermophysiscal properties yields a more reliable prediction, the constant properties model can yield similar prediction if a proper averaging parameter is chosen for each evaporating condition. In other words, there may exist an optimal value of the averaging parameter, for each evaporating condition, that allows consistent predictions by the constant parameter model, which is undoubtedly simpler to use than the one proposed here. Evaporating conditions are summarised by the Spalding mass transfer number $B_M = \frac{\chi_s^{(1)} - \chi_\infty^{(1)}}{1 - \chi_s^{(1)}}$, then a function $\alpha_{ref}\left(B_M\right)$, which can be used to calculate the thermophysical properties in the constant properties model, may exist to minimise the difference between the prediction of the two models.

A similar approach was already proposed in [30], when comparing the variable density model with the classical one, and the following similar expression for $\alpha_{ref}\left(B_M\right)$:

$$\alpha_{ref} = \frac{A_{\alpha_{ref}}}{\log\left(1+B_M\right)} + \frac{1}{1-\left(1+B_M\right)^{\frac{1}{A_{\alpha_{ref}}}}} \tag{35}$$

will be used here. The coefficient $A_{\alpha_{ref}}$ may depend on the drop species and the gas temperature, and it will be calculated minimising the overall discrepancies between the two models, i.e. by finding $A_{\alpha_{ref}}$ that minimises the following integral:

$$\int_0^{B_{M,\max}} \left|\gamma\left(B_M, A_{\alpha_{ref}}\right) - 1\right|^2 dB_M \tag{36}$$

Figure 4(a,b) reports the value of the evaporation ratio γ as a function of the Spalding mass transfer number B_M for three cases: $\alpha_{ref} = 1/2$, $\alpha_{ref} = 1/3$ and α_{ref} given by equation (35), for water drop vaporising in air at 500 K and 1000 K. The results confirm that at low/moderate evaporating conditions the use of $\alpha_{ref} = 1/2$ in the constant properties model yields good agreement with the model accounting for temperature dependence of the gas properties, while the use of $\alpha_{ref} = 1/3$ should be preferred for high evaporation conditions. However, increasing the gas temperature from 500K to 1000K increases the discrepancies that can be as large as 20%. The use of α_{ref} given by equation (35) (see again Figure 4a,b) with $A_{\alpha_{ref}} = 0.752$, as reported in Table 1, yields a much better agreement over all the range of evaporating conditions, with a maximum discrepancy of about 3%.

Figure 4(c,d) shows the corresponding graphs for n-dodecane. The use of a constant averaging parameter $\alpha_{ref} = 1/2$ leads to discrepancies of the order of 50% at 500 K and 1000 K, and similarly for the use of $\alpha_{ref} = 1/3$, which yields differences of the order of 35%. Again, when α_{ref} is calculated from the equation (35), using $A_{\alpha_{ref}}$ equal to 0.545 and 0.54 for gas temperature equal to 500 K and 1000 K, respectively, the maximum difference between the

two models is about 4%.

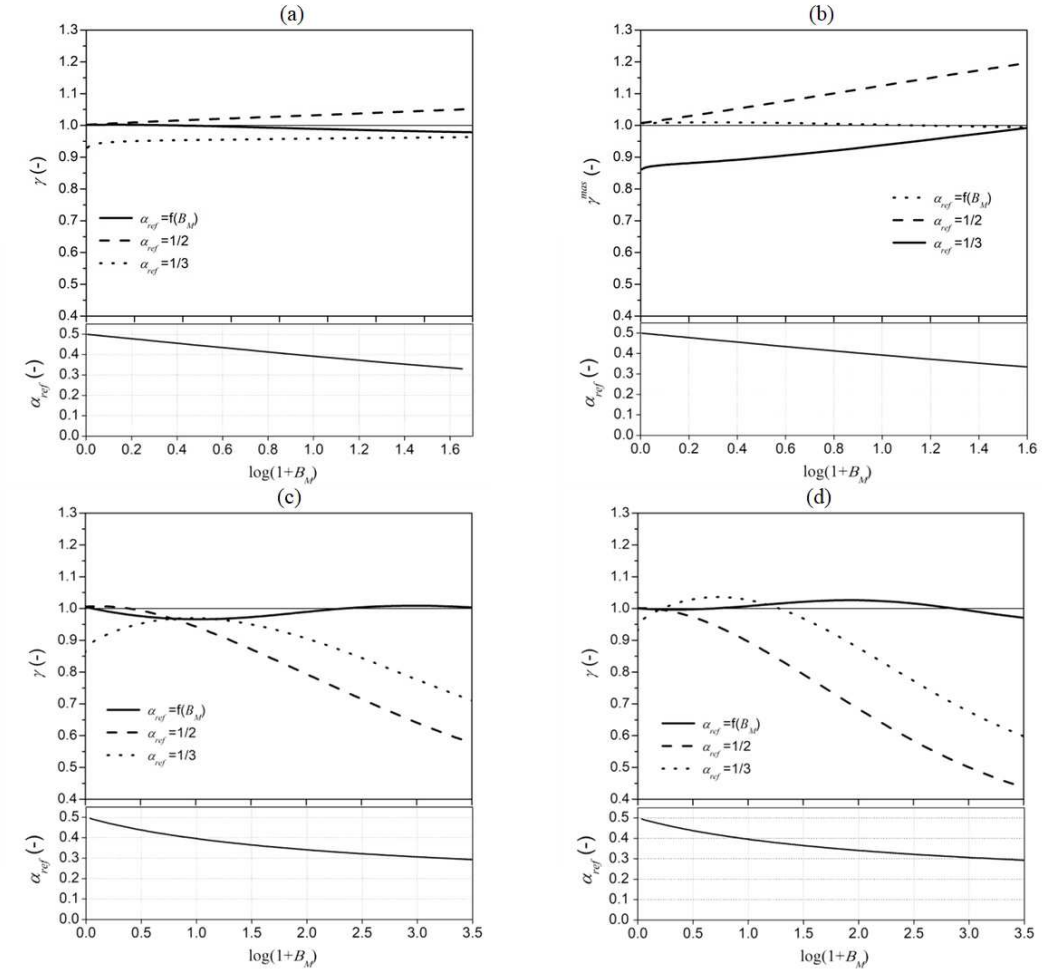

Figure 4. Evaporation rate ratio γ as function of the Spalding mass transfer number, calculated using α_{ref} from equation (35) (solid line), α_{ref} equal to 1/2 (dashed line) and α_{ref} equal to 1/3 (dotted line), water drop in air at (a) 500K and (b) 1000 K, and for n-dodecane drop in air at (c) 500 K and (d) 1000 K. The bottom graphs report equation (35).

The same analysis was repeated for some selected species (acetone, ethanol, n-hexane, n-octane) and the values of the constant $A_{\alpha_{ref}}$ found by the above described minimisation procedure are reported in table 3 for all the selected species and the two gas temperatures.

Table 3.

Values of the averaging constant $A_{\alpha_{ref}}$ (eq.35), for the six species and two operating conditions.

species	$T_\infty = 500K$	$T_\infty = 1000K$
water	0.752	0.752
acetone	0.753	1.24
ethanol	0.85	0.68
n-hexane	0.66	0.75
n-octane	0.6	0.65
n-dodecane	0.545	0.54

In these cases the maximum differences obtained using the variable average coefficient can be appreciated in figure 5. For all the selected species, the maximum discrepancy is lower than 4%.

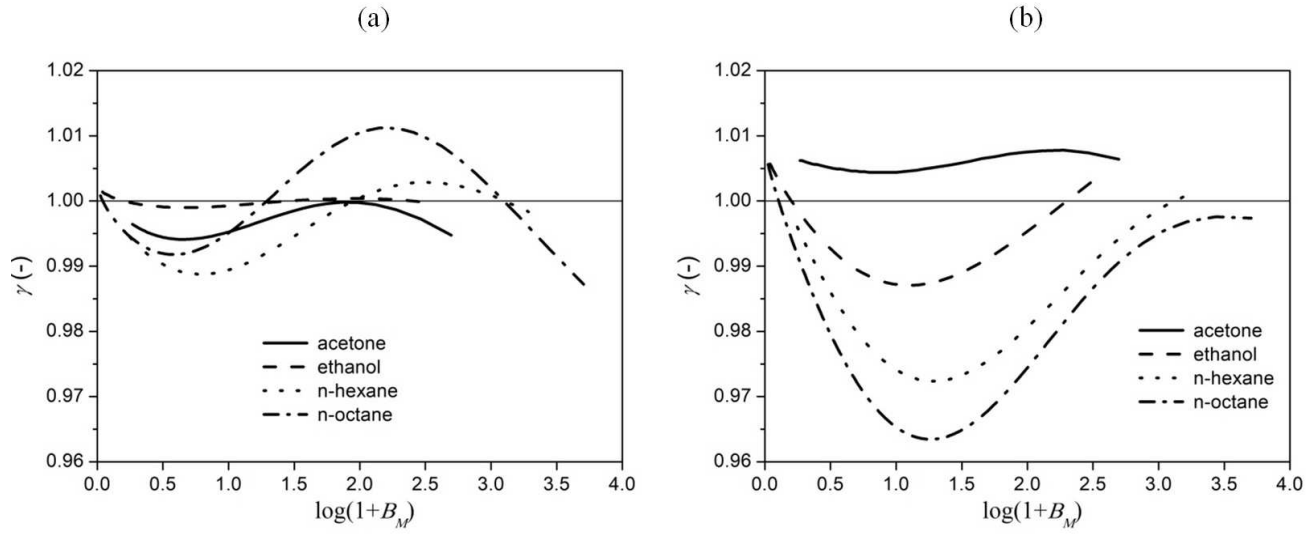

Figure 5. Evaporation rate ratio γ, as function of the Spalding mass transfer number, calculated using α_{ref} from equation (35), for different drop species evaporating in air at (a) 500 K and (b) 1000 K.

The extension of the reported model to convective conditions can be done by applying the film theory approach [2]. A diffusional region (film) is defined around the evaporating surface and a matching between the diffusional solution in the film with the free flow conditions is obtained by imposing the conditions on the region boundaries instead that at infinity. Although this extension is not reported here, preliminary analysis suggests that the ratio between the evaporation rates evaluated by the present model and by the constant properties model is only weakly affected and the results above reported may be extendable to convective conditions.

5 Conclusions

The developed model, capable to account for the temperature dependence of density, diffusivity, specific heat and thermal conductivity of the gas species, allows an analytical definition of the gas temperature and vapour distribution, in implicit form, and the direct evaluation of evaporation and heat rates as well as local fluxes in case of deformed drops.

The results can be extended, in analytic form, to any drop shape for which an analytical solution of the Laplace equation with uniform Dirichlet boundary conditions is available, and an example for the case of spheroidal drops is shown.

The present model is virtually independent of reference temperature and the comparison with the predictions of the classical constant property model evidences, as already pointed out by other researchers, the important effect of the reference temperature on the latter.

An analysis performed using the developed model on different evaporating species (water, ethanol, acetone, n-hexane, n-octane, n-dodecane) shows that a proper choice of the reference temperature as a function of the operating conditions may greatly improve the predictions of the classical model, and a way to evaluate an optimal value for the averaging parameter is reported.

A Appendix

The solution of the non-linear PDE system set by equations (21a, 21b) with uniform boundary conditions at infinity and on the drop surface can be found by introducing an auxiliary harmonic function Φ (i.e. $\nabla^2\Phi = 0$), zero at infinity and equal to 1 on the drop surface. This function depends only on the geometry of the drop surface while it is independent of the thermophysical properties and operating conditions.

To simplify the notation, define:

$$W_g(z) = {}_2F_1(g, 1, 1+g, z) \tag{A.1}$$

where ${}_2F_1(a, b, c, z)$ is the hypergeometric function [46]. The function W_g is the solution to the hypergeometric differential equation:

$$z(1-z)W_g'' + [1+g-(g+2)z]W_g' - gW_g = 0 \tag{A.2}$$

and satisfies the identity:

$$zW_g' + gW_g = \frac{g}{1-z} \tag{A.3}$$

In fact, setting $A(z) = zW_g' + gW_g$, equation (A.2) can be written as:

$$(1-z)A'(z) = A(z) \tag{A.4}$$

and the general solution is:

$$A(z) = \frac{C}{1-z} \tag{A.5}$$

From the properties of the hypergeometric function $W_g(0)=1$, then $A(0)=g$, yielding $C=g$ and (A.3) is proven. The function $\hat{H}$ is explicitly defined as a function of temperature as:

$$\hat{H}=-\frac{1}{K_0}\left[\frac{a_0\hat{T}^{q_0-m+2}}{h_0}W_{h_0}\left(\frac{\hat{T}^{1+b}}{K_0}\right)+\frac{a_1\hat{T}^{q_1-m+2}}{h_1}W_{h_1}\left(\frac{\hat{T}^{1+b}}{K_0}\right)\right]+\hat{H}_0 \tag{A.6}$$

where $h_p=\frac{2+q_p-m}{1+b}$, while K_0 and $\hat{H}_0$ are defined by the boundary conditions on the surface ($\hat{T}=\hat{T}_s$ and $\hat{H}=\hat{H}_s$) and at infinity ($\hat{T}=1$ and $\hat{H}=\hat{H}_\infty$):

$$\hat{H}_\infty=-\frac{1}{K_0}\left[\frac{a_0}{h_0}W_{h_0}\left(\frac{1}{K_0}\right)+\frac{a_1}{h_1}W_{h_1}\left(\frac{1}{K_0}\right)\right]+\hat{H}_0 \tag{A.7a}$$

$$\hat{H}_s=-\frac{1}{K_0}\left[\frac{a_0\hat{T}_s^{q_0-m+2}}{h_0}W_{h_0}\left(\frac{\hat{T}_s^{1+b}}{K_0}\right)+\frac{a_1\hat{T}_s^{q_1-m+2}}{h_1}W_{h_1}\left(\frac{\hat{T}_s^{1+b}}{K_0}\right)\right]+\hat{H}_0 \tag{A.7b}$$

The function $\hat{T}$ is implicitly defined by the relationship with Φ as:

$$\Phi=\Phi_1\left[a_0\frac{\hat{T}^{q_0+1}\ W_{g_0}\left(\frac{\hat{T}^{1+b}}{K_0}\right)}{K_0(q_0+1)}+a_1\frac{\hat{T}^{q_1+1}\ W_{g_1}\left(\frac{\hat{T}^{1+b}}{K_0}\right)}{K_0(qp_1+1)}\right]+\Phi_0 \tag{A.8}$$

where $g_p=\frac{1+q_p}{1+b}$, while Φ_1 and Φ_0 are defined by the boundary conditions on the surface ($\hat{T}=\hat{T}_s$ and $\Phi=1$) and at infinity ($\hat{T}=1$ and $\Phi=0$):

$$1=\Phi_1\left[a_0\frac{\hat{T}_s^{q_0+1}\ W_{g_0}\left(\frac{\hat{T}_s^{1+b}}{K_0}\right)}{K_0(q_0+1)}+a_1\frac{\hat{T}_s^{q_1+1}\ W_{g_1}\left(\frac{\hat{T}_s^{1+b}}{K_0}\right)}{K_0(q_1+1)}\right]+\Phi_0 \tag{A.9a}$$

$$0=\Phi_1\left[a_0\frac{W_{g_0}\left(\frac{1}{K_0}\right)}{K_0(q_0+1)}+a_1\frac{W_{g_1}\left(\frac{1}{K_0}\right)}{K_0(q_1+1)}\right]+\Phi_0 \tag{A.9b}$$

To notice that only the evaluation of K_0 needs the solution of a non-linear trascendental equation, obtained form (A.7a) and (A.7b) after eliminating $\hat{H}_0$, while the other constants ($\hat{H}_0$, Φ_1, Φ_0) are found by solving linear algebraic equations. That the functions $\hat{H}$ and $\hat{T}$ are solutions of the non-linear PDE system (21a) and (21b) is proven as follows. First calculate the gradients:

$$\nabla_j\hat{H} = -\left[a_0\nabla_j\left[\frac{\hat{T}^{q_0-m+2}}{K_0h_0}W_{h_0}\left(\frac{\hat{T}^{1+b}}{K_0}\right)\right]+a_1\nabla_j\left[\frac{\hat{T}^{q_1-m+2}}{K_0h_1}W_{h_1}\left(\frac{\hat{T}^{1+b}}{K_0}\right)\right]\right] \tag{A.10a}$$

$$\nabla_j\Phi = \Phi_1\left[a_0\nabla_j\left[\frac{\hat{T}^{q_0+1}\ W_{g_0}\left(\frac{\hat{T}^{1+b}}{K_0}\right)}{K_0(q_0+1)}\right]+a_1\nabla_j\left[\frac{\hat{T}^{q_1+1}\ W_{g_1}\left(\frac{\hat{T}^{1+b}}{K_0}\right)}{K_0(q_1+1)}\right]\right] \tag{A.10b}$$

Using the identity (A.3):

$$\nabla_j\left[\frac{\hat{T}^{q_0-m+2}}{K_0h_0}W_{h_0}\left(\frac{\hat{T}^{1+b}}{K_0}\right)\right] = \frac{\hat{T}^{q_0-m+1}(b+1)}{K_0h_0}\left[h_0W_{h_0}\left(\frac{\hat{T}^{1+b}}{K_0}\right)+\frac{\hat{T}^{1+b}}{K_0}W'_{h_0}\left(\frac{\hat{T}^{1+b}}{K_0}\right)\right]\nabla_j\hat{T}= \tag{A.11a}$$

$$= \frac{\hat{T}^{q_0-m+1}(1+b)}{K_0-\hat{T}^{1+b}}\nabla_j\hat{T}$$

$$\nabla_j\left[\frac{\hat{T}^{q_0+1}\ W_{g_0}\left(\frac{\hat{T}^{1+b}}{K_0}\right)}{K_0(q_0+1)}\right] = \frac{\hat{T}^{q_0}(b+1)}{K_0(q_0+1)}\left[g_0\ W_{g_0}\left(\frac{\hat{T}^{1+b}}{K_0}\right)+\frac{\hat{T}^{1+b}}{K_0}W'_{g_0}\left(\frac{\hat{T}^{1+b}}{K_0}\right)\right]\nabla_j\hat{T}= \tag{A.11b}$$

$$= \frac{\hat{T}^{qp_0}}{K_0-\hat{T}^{1+b}}\nabla_j\hat{T}$$

then:

$$\nabla_j \hat{H} = -\left[a_0 \hat{T}^{q_0} + a_1 \hat{T}^{q_1}\right] \frac{\hat{T}^{1-m}\,(1+b)\,\nabla_j \hat{T}}{K_0 - \hat{T}^{1+b}} \tag{A.12a}$$

$$\nabla_j \Phi = \Phi_1 \left[a_0 \hat{T}^{q_0} + a_1 \hat{T}^{q_1}\right] \frac{\nabla_j \hat{T}}{K_0 - \hat{T}^{1+b}} \tag{A.12b}$$

and consequently:

$$\hat{T}^{m-1} \nabla_j \hat{H} = -\frac{(1+b)}{\Phi_1} \nabla_j \Phi \tag{A.13}$$

which shows that equation (21a) $\nabla_j \left(\hat{T}^{m-1} \nabla_j \hat{H}\right) = 0$ is satisfied since $\nabla^2 \Phi = 0$. Using equation (A.13), the LHS of equation (21b) can be written as:

$$\left(\hat{T}^{m-1+b} \nabla_j \hat{H}\right) \nabla_j T = -\hat{T}^b \frac{(1+b)}{\Phi_1} \nabla_j \Phi \nabla_j T \tag{A.14}$$

whereas using equation (A.12a) the RHS becomes:

$$\nabla_j \left[\left(a_0 \hat{T}^{q_0} + a_1 \hat{T}^{q_1}\right) \nabla_j T\right] = \frac{1}{\Phi_1} \nabla_j \left[\left(K_0 - \hat{T}^{1+b}\right) \nabla_j \Phi\right] = -\hat{T}^b \frac{(1+b)}{\Phi_1} \nabla_j \hat{T} \nabla_j \Phi \tag{A.15}$$

proving that also equation (21b) is satisfied.

A.1 Some computational issues

The functions $W_g\left(\frac{z}{K_0}\right) = {}_2F_1\left(g, 1, 1+g, \frac{z}{K_0}\right)$ are real for $K_0 < z$ (z is always positive), the limit: $\lim_{K_0 \to z^-} W_g\left(\frac{z}{K_0}\right)$ is infinite and the function becomes complex when $K_0 > z$. Since the value of K_0 is given by the equations (A.7b, A.7a), the assumption that K_0 must be real implies that $K_0 < \hat{T}_s^{1+b}$. The constant K_0 is found by solving the trascendent equation (22) that contains the functions: $W_{h_p}\left(\frac{\hat{T}^{1+b}}{K_0}\right), W_{h_p}\left(\frac{1}{K_0}\right)$,and when $K_0 > 0$, since $\frac{1}{K_0} > \frac{\hat{T}_s^{1+b}}{K_0} > 1$, the functions become complex valued. For such conditions it was found convenient to use equation 15.8.2 of [46] to transform the functions as:

$$W_h\left(\frac{z}{K_0}\right) = F\left(h, 1, 1+h, \frac{z}{K_0}\right) = \left\{ \begin{array}{c} \Gamma(1-h)\,\Gamma(1+h)\left(-\frac{z}{K_0}\right)^{-h} F\left(h, 0, h, K_0/z\right) \\ +\frac{\Gamma(1-h)h}{\Gamma(2-h)}\left(\frac{z}{K_0}\right)^{-1} F\left(1-h, 1, 2-h, K_0/z\right) \end{array} \right\} \tag{A.16}$$

so that the hypergeometric functions that appear in the calculations are real valued. It is worth to notice that function W_h can be written also in term of the incomplete Beta function [46]:

$$W_h(z) = {}_2F_1(h, 1, 1+h, z) = z^{-h} B(z, h, 0)\, h \tag{A.17}$$

which can be used to write equations (21a, 21b) in simpler form. The incomplete Beta function admits the following integral form:

$$B(z, h, 0) = \int_0^z \frac{t^{h-1}}{1-t} dt \tag{A.18}$$

which can be used to show, in a relatively straightforward way, that the solutions (21a, 21b) are finite when $K_0 \to 0$.

References

[1] Z. Zhifu, W. Guoxiang, C. Bin, G. Liejin, W. Yueshe, Powder Technol. 240 (2013) 95-102.

[2] S.S. Sazhin, Droplet and Sprays, Springer, 2014.

[3] G. Strotos, I. Malgarinos, N. Nikolopoulos, M. Gavaises, Predicting the evaporation rate of stationary droplets with the VOF methodology for a wide range of ambient temperature conditions, Int. J. Thermal Sciences 109 (2016) 253-262.

[4] J.C. Maxwell, Diffusion, Ency. Brit., 9th ed., VII, 1877, pp. 214–221.

[5] N.A. Fuchs, Vaporisation and Droplet Growth in Gaseous Media, Pergamon Press, London, 1959.

[6] G.L. Hubbard, V.E. Denny, A.F. Mills, Droplet evaporation: effects of transients and variable properties, Int. J. Heat Mass Transfer 18 (1975) 1003–1008.

[7] B. Abramzon, W.A. Sirignano, Droplet vaporization model for spray combustion calculations, Int. J. Heat Mass Transfer 32 (9) (1989) 1605–1618.

[8] R.S. Miller, K. Harstad, J. Bellan, Evaluation of equilibrium and non-equilibrium evaporation models for many -droplet gas-liquid flow simulations, Int. J. Multiphase Flow 24 (6) (1998) 1025–1055.

[9] M. Sanjosé, Evaluation de la méthode Euler-Euler pour la simulation numérique aux grandes échelles des chambres à carburant liquide, Phd thesis, INP Toulouse, 2009.

[10] V. Ebrahimian, C. Habchi, Towards a predictive evaporation model for multi-component hydrocarbon droplets at all pressure conditions, Int. J. Heat Mass Transfer 54 (15-16) (2011) 3552-3565.

[11] R.T. Imaoka, W.A. Sirignano, Transient vaporisation and burning in dense droplet spray, Int. Journal Heat Mass Transfer 48 (2005) 4354-4366.

[12] B. Sobac, P. Talbot, B. Haut, A. Rednikov, P. Colinet, A comprehensive analysis of the evaporation of a liquid spherical drop, Journal Colloid and Interface Science 438 (2015) 306-317.

[13] S. Tonini, G.E. Cossali, An analytical model of liquid drop evaporation in gaseous environment, Int. J. Thermal Sciences 57 (2012) 45-53.

[14] G.E. Cossali, S. Tonini, Variable gas density effects on transport from interacting evaporating spherical drops, Int. J. Heat Mass Transfer 127 (2018) 485-496.

[15] G.E. Cossali, S. Tonini, Modelling the effect of variable density and diffusion coefficient on heat and mass transfer from a single component spherical drop evaporating in high temperature air streams, Int. Journal Heat Mass Transfer 118 (2018) 628-636.

[16] D. de Oliveira Maionchi, F. Fachini Filho, An exact solution for droplet vaporisation with variable transport coefficients, 22^{nd} International Congress of Mechanical Engineering (COBEM 2013), Ribeirão Preto, SP, Brazil, 3-7 November 2013.

[17] J. Qian, C.K. Law, Regimes of coalescence and separation in droplet collision, Journal Fluid Mechanics 331 (1997) 59-80.

[18] M. Birouk, S.C. Fabbro, Droplet evaporation in a turbulent atmosphere at elevated pressure – experimental data, Proc. Combust. Inst. 34 (1) (2013) 1577–1584.

[19] F. Mashayek, Dynamics of evaporating drops. Part I:formulation and evaporation model, Int. J. Heat Mass Transfer 44 (2001) 1517–1526.

[20] E. Loth, Quasi-steady shape and drag of deformable bubbles and drops, Int. J. Multiph. Flow 34 (6) (2008) 523–546.

[21] M. Dai, J.B. Perot, D.P. Schmidt, Heat transfer within deforming droplets, Proc. ASME 1 (2002) 1-6.

[22] R. Clift, J.R. Grace, M.E. Weber, Bubbles, Drops and Particles, Academic Press, New York, 1978.

[23] B. Al Zaitone, Oblate spheroidal droplet evaporation in an acoustic levitator, Int. J. Heat Mass Transfer 126 (2018) 164-172.

[24] G.A.E. Godsave, Studies of the Combustion of Drops in a Fuel Spray: The Burning of Single Drops of Fuel, Fourth Symposium (International) on Combustion, Williams and Wilkins, Baltimore, pp. 818-830, 1953.

[25] P.J. Sáenz, A.W. Wray, Z. Che, O.K. Matar, P. Valluri, J. Kim, K. Sefiane, Dynamics and universal scaling law in geometrically-controlled sessile drop evaporation. Nature communications 8 (2017): 14783.

[26] R. Kumar, E. Tijerino, A. Saha, S. Basu, Structural morphology of acoustically levitated and heated nanosilica droplet, Appl. Phys. Lett. 97 (12) (2010) 123106.

[27] S. Tonini, G. Cossali, An exact solution of the mass transport equations for spheroidal evaporating drops, Int. J. Heat Mass Transfer 60 (2013) 236–240.

[28] S. Tonini, G.E. Cossali, One-dimensional analytical approach to modelling evaporation and heating of deformed drops. Int J Heat Mass Transfer 9 (2016) 301–307.

[29] S. Tonini, G.E. Cossali, An analytical approach to model heating and evaporation of multicomponent ellipsoidal drops, Heat and Mass Transfer (2018) DOI: 10.1007/s00231-018-2511-3 (in press).

[30] S. Tonini, G.E. Cossali, On molar- and mass-based approaches to single component drop evaporation modelling, Int. Communications Heat Mass Transfer 77 (2016) 87-93.

[31] V.S. Zubkov, G.E. Cossali, S. Tonini, O. Rybdylova, C. Crua, M. Heikal, S.S. Sazhin, Mathematical modelling of heating and evaporation of a spheroidal droplet, Int. J. Heat Mass Transfer 108 (2017) 2181–2190.

[32] J.C. Slattery, Momentum, Energy and Mass Transfer in Continua, second ed., R. Krieger Publ., New York, 1981.

[33] R. Bird, W. Stewart, E. Lightfoot, Transport Phenomena, second ed., John Wiley and Sons, 2002.

[34] G.H. Wannier, Statistical Physics, J.W. & Sons, 1966.

[35] E.N. Fuller, P.D. Schetter, J.C. Giddings, New method for prediction of binary gas-phase diffusion coefficients, Industrial Engineering Chemistry 58 (5) (1966) 18-27.

[36] J.O. Hirschfelder, C.F. Curtiss, R.B. Bird, Molecular Theory of Gases and Liquids, Wiley, New York, 2nd corrected printing (1964) p. 534.

[37] J.H. Ferziger, H.G. Kaper, Mathematical Theory of Transport Processes in Gases, North-Holland, Amsterdam, 1972.

[38] A. Wassiljewa, Heat Conduction in Gas Mixtures, Physikalische Zeitschrift 5 (22) (1904) 737-742.

[39] A.L. Lindsay, L.A. Bromley, Thermal Conductivity of. Gas Mixtures, Ind. Eng. Chem. 42 (1950) 1508-1511.

[40] H.J. Bernstein, Power Series for the Temperature Dependence of the Heat Capacity of Gases, J. Chemical Physics 24 (1956) 911-912.

[41] E.W. Lemmon, M.L. Huber, M.O. McLinden, NIST Standard Reference Database 23: Reference Fluid Thermodynamic and Transport Properties-REFPROP, Version 8.0, National Institute of Standards and Technology, Standard Reference Data Program, Gaithersburg, 2007.

[42] D. Misic, G. Thodos, The thermal conductivity of hydrocarbon gases at normal pressures, AIChE Journal 7 (2) (1961) 264-267.

[43] S. Tonini, G.E. Cossali, A novel vaporisation model for a single-component drop in high temperature air streams, Int. J. Therm. Sci. 75 (2014) 194–203.

[44] M. Labowsky, A formalism for calculating the evaporation rates of rapidly evaporating interacting particles, Combust Sci Technol 18 (1978) 145-151.

[45] A. Umemura, S. Ogawa, N. Oshima, Analysis of the interaction between two burning droplets, Combust Flame 41 (1981) 45-55.

[46] F.W.J. Olver, D.W. Lozier, R.F. Boisvert, C.W. Clark, The NIST Handbook of Mathematical Functions, Cambridge Univ. Press, 2010.

[47] P. Moon, D.E. Spencer, Field Theory Handbook, Springer-Verlag, Heidelberg, 1988.

[48] M.C. Yuen, L.W. Chen, On drag of evaporating droplets, Combust. Sci. Technol. 14 (1976) 147–154.

B List of Figures

Figure 1: Effect of averaging parameter α_{ref} on the evaporation rate ratio predicted by the constant property model, as function of drop temperature at two gas temperatures, for (a) water and (b) n-dodecane drop.

Figure 2: Effect of averaging parameter α_{ref} on the evaporation rate ratio predicted by the present variable property model, as function of drop temperature at two gas temperatures, for (a) water and (b) n-dodecane drop.

Figure 3: Evaporation rate ratio γ as function of liquid temperature, for different averaging parameter α_{ref} in the constant gas density model, for water drops at (a) 500 K and (b) 1000 K gas temperature and for n-dodecane drops at (c) 500 K and (d) 1000 K gas temperature.

Figure 4: Evaporation rate ratio γ, as function of the Spalding mass transfer number, calculated using α_{ref} from equation (35) (solid line), α_{ref}=1/2 (dashed line) and α_{ref}=1/3 (dotted line), for water drop in air at (a) 500 K and (b) 1000 K, and for n-dodecane drop in air at (c) 500 K and (d) 1000 K. The bottom graphs report equation (35).

Figure 5: Evaporation rate ratio γ, as function of the Spalding mass transfer number, calculated using α_{ref} from equation (35), for different drop species evaporating in air at (a) 500 K and (b) 1000 K.